

Continuous Flow Synthesis of Ceria Nanoparticles Using Static T-mixers

Barath Palanisamy and Brian Paul

Oregon State University

Abstract

Ceria nanoparticles are of interest owing to their interesting properties like photo-absorption and ability to absorb oxygen. Several batch synthesis routes exist however these methods often lack particle size control, result in agglomeration and typically require high temperature processing. In this paper, a continuous flow microchannel synthesis method based on precipitation is demonstrated with a static T-mixer, showing improved size control without agglomeration through the manipulation of flow parameters. Three flow rates were chosen representing different mixing modes and computational fluid dynamics simulations were used to visualize flow conditions. The nanoparticles were characterized for composition, size and size distribution using transmission electron microscopy, wave dispersive spectroscopy and x-ray diffraction. The engulfment flow condition, corresponding to the highest Reynolds number in this study, gave the narrowest particle size distribution (15.0 ± 4.7 nm) and best compositional uniformity.

Introduction

Cerium oxide (CeO_2) has been widely investigated due to its distinctive characteristics in UV absorptivity [1] and high reactivity to oxygen [2]. More recently, the size-induced property changes of ceria nanoparticles (NPs) have led to reductions in response times within oxygen sensors [1] and decreases in sintering temperatures [2]. Cerium oxide NPs have been proposed as a substitute for silica in chemical mechanical planarization (CMP) owing to its higher hardness and better material removal characteristics [3]. Other applications for ceria NPs include radical scavenging [4], catalysis [5], sintering [6], solid oxide fuel cells [7, 8] and in sunscreens due to the UV absorbing properties [9]. Attributes of importance for these applications include narrow size distribution, shape, crystallinity and deagglomeration of nanoparticles.

Several approaches exist in the technical literature for the synthesis of ceria nanoparticles. Most batch chemistries involve a cerium salt like nitrate or chloride or acetate which is then reduced by a base like ammonium hydroxide or sodium hydroxide or amines. It has been found that pH is a critical variable for the synthesis of ceria and can affect the particle formation [10]. Depending on the solvent used (water/alcohol) and the reactant combination, the morphology of the particles has been demonstrated to vary from spheres to cubes and rods. Hydrothermal processing typically involves reacting cerium salts at high temperatures and pressures to create a gel precursor consisting of a cerium salt complex and drying precipitates in an oxygen environment [11]. Using cerium nitrate and sodium hydroxide, Mai *et al* produced ceria nanoparticles in various morphologies including spheres, cubes and rods by changing the base concentration and

the hydrothermal processing temperature [12]. Microemulsion is another route that has been demonstrated for the synthesis of ceria nanoparticles. Rebellato et al successfully produced ceria of average size 3 nm though the particles appear to have wide size distributions and low crystallinity [8]. Electrochemical deposition has been used to yield 20 nm diameter ceria nanoparticles, however, additional heat treatment at 650 °C was used to improve the crystallinity. The process also involves tedious process control and equipment maintenance [13]. Sonochemical synthesis is yet another route characterized by long processing times (several hours) and agglomerated nanoparticles [14]. Despite the many routes for ceria synthesis, control over particle, size, crystallinity and agglomeration during synthesis remain a challenge.

For many applications, precipitation is an attractive route to ceria NP synthesis due to the cheap salt precursors, simple operation, and ease for mass production [15, 16]. However, traditional precipitation approaches in batch reactors often face long cycle times and difficulties in controlling particle size due to poor heat and mass transfer. Due to these same transport issues, batch reactors are difficult to scale to production volumes. Microchannel reactors offer accelerated heat and mass transfer which allows for rapid changes in reaction temperatures and concentrations leading to more uniform heating and mixing [17]. During nucleation, microchannel mixers offer the possibility of reducing mixing times through shorter diffusional distances and, in some cases, advective assistance. Edel et al were able to reduce the mixing time for the synthesis of CdS to the order of milliseconds by utilizing microchannels [18]. During NP growth, microchannel reactors are attributed to facilitating better control over reaction temperature and residence time [19]. Consequently, microreactors have been demonstrated to have dramatic impacts on macromolecular yields [20, 21] and nanoparticle size distributions [22-25]. The cycle time advantages of using a static microchannel T-mixer for the synthesis of ceria nanoparticles was demonstrated by Tseng et al [26]. The objective of this paper is to investigate the effects of flow conditions and flow chemistry within a static microchannel T-mixer on the size, size distribution, crystallinity and agglomeration of ceria nanoparticles.

Flow Conditions

In static microchannel T-mixers, two reactant fluids are injected into the two inlets at a constant flow rate and the fluids are mixed within an outlet channel. The flow is typically laminar with Reynolds numbers (Re) not generally exceeding 1000. Three dominant kinds of flow have been observed [27]. At a Re of less than 50, the fluid streams are stratified resulting in diffusion-controlled mixing which is relatively slow. As Re increases, vortices begin to occur within the flow along a plane of symmetry about the axis of the outlet [28]. As the Re approaches about 240, engulfment flow begins to occur characterized by the fluid streams crossing over the central plane providing the best mixing conditions in this regime. Several researchers have validated these flow regimes using CFD simulations and experiments for microchannels with square and rectangular cross-sections [27, 29, 30]. However many off-the-shelf static T-mixers have circular cross-sections.

Numerical simulations were performed for the actual geometry of the T-mixer used in the experiments to help visualize mixing conditions within the circular mixing channel. A 3D model was created using Gambit 2.4.6 and imported into ANSYS Fluent 12.1 for solving mass and momentum conservation equations. Results were exported after convergence and are shown in Figure 1. Figure 1a shows the cross-section of flow in the outlet near the end of the flow as

shown in Figure 1b. The images in Figure 1b show the two fluids flowing through inlets from the left and right and into an outlet on the top. As shown, the mixing conditions change from a diffusion-limited, stratified flow to a diffusion-enhanced, advective flow. In the case of the lowest Re (40), it can be seen that there is no cross-over resulting only in diffusional mixing at the liquid-liquid interface. At a Re of 245, the fluid streams begin to cross-over indicating the onset of engulfment flow. At a Re of 325, it is clear that the fluid streams have intimate mixing due to engulfment flow. These Re are similar to those reported in the literature for the onset of engulfment flow [27, 29, 30].

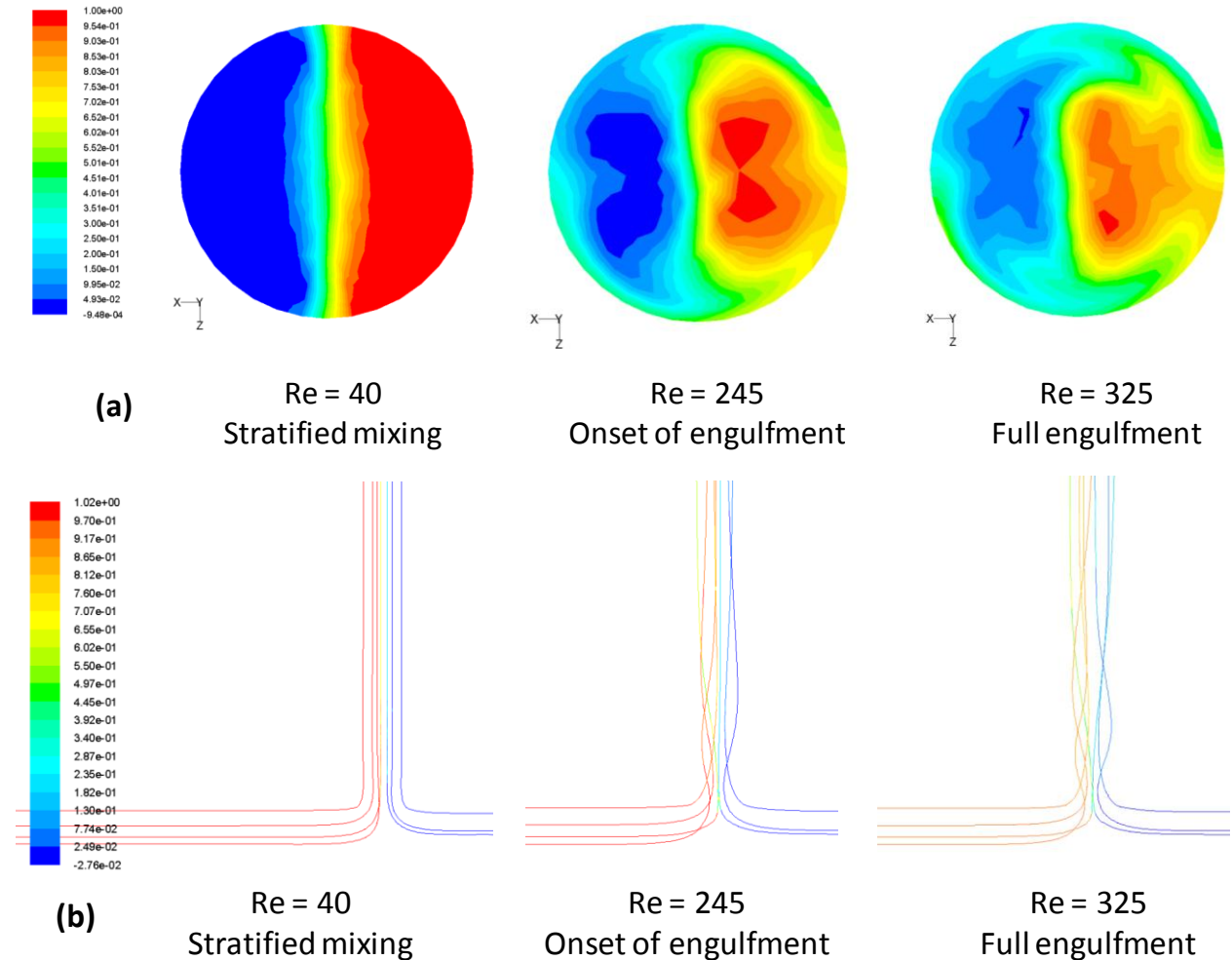


Figure 1: Flow transition in static T-mixer observed in CFD numerical simulation

(a) Contour map of species mass fraction near outlet – cross section/top view

(b) Streamlines colored by species mass fraction – front view

While engulfment flow in T-shaped microchannel mixers has been shown to provide better mixing characteristics [27-30], very little work has been reported to date on exploiting these findings for nanoparticle synthesis [31, 32]. Further, prior research with static T-mixers studying the effect of engulfment flow on particle size did not investigate the effects of engulfment on

agglomeration or crystallinity [31]. Other researchers have evaluated the effect of mixing conditions beyond engulfment at Re up to 8000 in the outlet of microchannel T-mixers [33-36]. While researchers have shown that increasing Re over 1000 can reduce the average particle size and the size dispersion, this has been achieved at very high fluid velocities [33, 34]. For instance, 60 nm BaSO₄ NPs were produced at a very high throughput of 300 ml/min with an average velocity of 6.4 m/s based on calculations [36]. At these high fluid velocities, slurry erosion of the channel walls becomes a concern especially during the synthesis of oxide nanoparticles which are generally very hard. Liu et al showed that significant erosion can arise in an oxide-reinforced metal (Ni) matrix composite at fluid velocities as low as 3 m/s [37]. In this study, the three flow conditions shown in Figure 1 were used to evaluate the effect of engulfment on ceria NP size, size distribution, crystallinity and agglomeration.

Flow Chemistry

Within precipitation reactions, particle size is affected by the nucleus size at nucleation which is in turn controlled by the supersaturation of reactants. For a precipitation reaction, particle nucleation occurs when the concentration of reactants become supersaturated. The effect of supersaturation on critical nuclei size has been explained by Mullin [38] for precipitation reactions and can be summarized in the following equation:

$$S = \frac{[Ce^{3+}][OH^{-}]^3}{K_{SP}} \dots\dots\dots(1)$$

where S is the supersaturation and K_{SP} is the solubility product and

$$r^* = \frac{2v\gamma}{kT \ln(S)} \dots\dots\dots(2)$$

where r* is the critical nuclei size, k is the Boltzmann constant, γ is the interfacial energy and v is the molecular volume for the compound. Based on Equation 2, it can be observed that higher supersaturation values can result in smaller nuclei and, therefore, smaller particles. In this paper, reactant concentrations of 0.09M were calculated to yield a nucleus diameter of 5 nm.

Prior batch precipitation chemistries have involved the reaction of cerium nitrate and ammonium hydroxide dissolved in a water-alcohol solvent. The pH of this reaction was not allowed to go beyond 8 and progressed at room temperature. Following synthesis, the particles were calcined at temperatures 500, 600, 700 and 800 °C and an associated improvement in crystallinity was observed [39]. The room temperature reaction of cerium nitrate and triethanolamine (TEA) in ethanol over 40 minutes has yielded ceria nanoparticles with nearly spherical morphology and a size distribution of 5.9 ± 0.5 nm. An intermediate Ce (IV)-TEA complex was found to promote the oxidation of Ce³⁺ to Ce⁴⁺ [40].

As a result, the flow chemistry proposed below was chosen to increase the rate of nucleation by increasing the rate of pH change. NaOH is proposed here as a stronger base for precipitation.

Also, TEA is used to aid the conversion of cerium salt to its oxide and it has also been reported to act as a surfactant for deagglomeration [41].

Experimental procedure

In this research, computational fluid dynamics (CFD) simulations were performed to identify the best mixing conditions and also to understand the fluid flow transitions occurring in flow in a microchannel T-mixer with a circular cross-section. Three flow rates (2.3, 15, 20 ml/min) were chosen representing the flow conditions shown in Figure 1. A Tygon® tube of inner diameter 1.22 mm and length 50 mm was added to the outlet of the T-mixer. Overall, based on flow rates and the mixer setup, average residence times for the three mixing conditions were calculated to be 1.6, 0.25 and 0.18 sec, respectively. A 500 µm diameter static T-mixer (IDEX Corp, USA) was used for the nanoparticle synthesis. Reagent solutions of 0.09M $\text{Ce}(\text{NO}_3)_3 \cdot 6\text{H}_2\text{O}$ and 0.09M NaOH were prepared using 2-propanol as a solvent. To further aid in the reaction and to act as a surfactant, 0.5M of TEA was added to the mixed solution. The reaction was quenched and the as-synthesized nanoparticles were collected after centrifuging at 12000 rpm and washed repeatedly before examination. A Harvard Apparatus PHD2000 Syringe pump (Holliston, MA, USA) was used to pump the reagents through the T-mixer at varying flow rates. All the experiments were performed within a controlled environment at 22°C.

A Phillips CM-12 TEM operating at 120 kV and a FEI TITAN TEM (Portland, OR, USA) operating at 300 kV were used to image the nanoparticles. A Bruker-AXS D8 Discover X-ray diffraction unit (Madison, WI, USA) was used for phase analysis using XRD patterns. A SX-100 CAMECA Electron microprobe analyzer (Gennevillier, France) was used to evaluate the composition of nanoparticles using wave dispersive spectroscopy. Simultaneous thermogravimetric analysis and differential scanning calorimetry were performed using a TA Instruments Q600 (New Castle, DE, USA) to study the thermally induced phase changes.

Results and discussion

Experiments were carried out by fixing the concentrations of the reactant while the flow rates were varied to realize the three different Reynolds numbers.

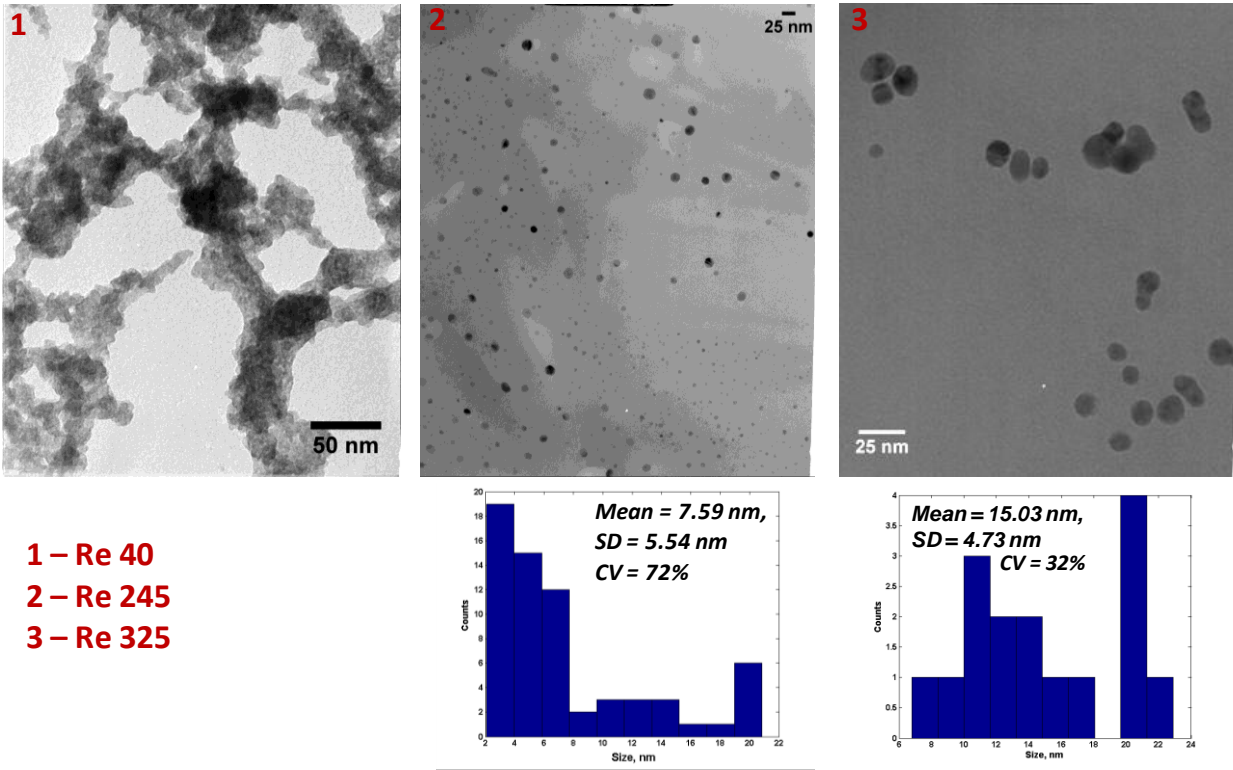


Figure 2: Nanoparticle size from TEM for a) Re = 40 b) Re = 245 c) Re = 325 and size distribution d) for image b and e) for image c

Figure 2 shows the corresponding experimental results after ceria nanoparticle synthesis. At a Re of 40, it can be observed that there is extensive agglomeration yielding structures with features approaching a micrometer in scale. At a Re of 245 at the onset of engulfment, interestingly the nanoparticles no longer appear agglomerated. The shape was found to be spherical with a wide coefficient of variance for particle size. At a Re of 325, it was observed that the particle size distribution is narrower and the shape remains unchanged with increasing Re. In addition, the average particle size was found to be larger owing to better mixing leading to higher supersaturation and higher growth rates in a diffusion controlled regime. This would also explain the marked absence of a population of smaller particles i.e. the distribution is skewed to the right unlike the case where Re = 245

X-ray diffraction patterns for the nanoparticles are shown in Figure 3. In Figure 3a, the presence of cerium hydroxide peaks in the diffraction pattern suggests that the reaction is incomplete. With increasing Re, the occurrence of these peaks is reduced. Based on integral area under the peaks for $\text{Ce}(\text{OH})_3$ which is indirectly affected by the wt% of this phase, a 40% reduction in occurrence of $\text{Ce}(\text{OH})_3$ for Re = 245 (3b) and a 75% reduction for Re = 325 (3c) is observed. This indicates completion of the reaction at higher Re even though the residence time for condition (b) is $1/6^{\text{th}}$ that for condition (a) and the residence time for condition (c) is $1/8^{\text{th}}$ that for

condition (a). This further supports the notion of enhanced mixing at higher Re. As Re increases, the additional peaks of ceria (311) and (400) appear due to the additional conversion of reactants and Ce(OH)₃ to CeO₂. This higher conversion is apparent by simply measuring the dry weight of obtained precipitates. The weights of the obtained precipitate for Re values of 40, 245 and 325 were 0.7 mg, 5.5 mg and 6.3 mg respectively. The XRD data was deconvoluted to separate the crystalline and amorphous phase contributions. Based on the intensities of the peaks the following formula was used to calculate the percentage crystallinity as outlined by He [42].

$$\text{Percentage crystallinity } X_C = \frac{I_c}{I_c + I_A} \times 100$$

Where I_C is intensity of the crystalline phase and I_A is the intensity of the amorphous phase. Based on this equation the values of X_C for Re 40, 245, 325 were found to be 26.5%, 27.3% and 37.7% respectively.

This suggests improved stoichiometry and crystallinity with increasing Re due to better mixing conditions. It is expected that the better mixing conditions led to a better stoichiometric distribution of reactants and hence higher crystallinity. In all cases, cerium hydroxide peaks were observed as an intermediate compound. It is well known that subsequent exposure to oxygen can convert the remaining hydroxide into oxide. Also observed were some unidentified peaks which were prominent in lower Re. These peaks could be possibly attributed to [Ce(TEA)₂(NO₃)](NO₃)₂ complex as mentioned by Pati et al during synthesis of ceria using TEA [41].

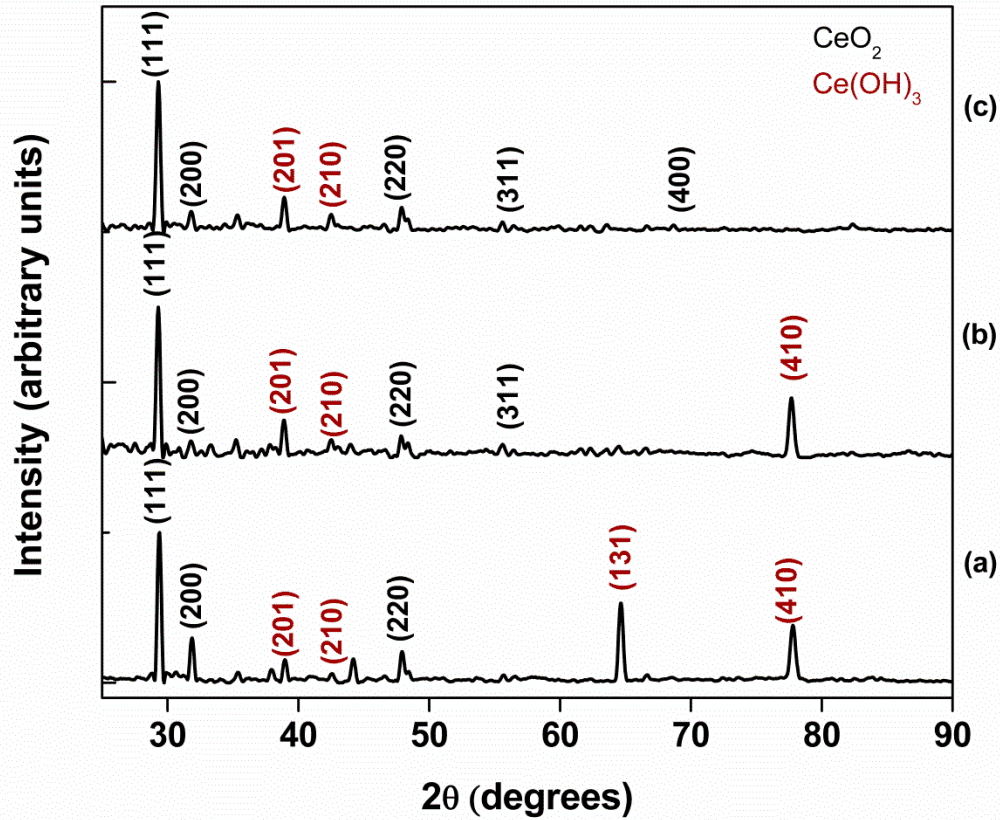


Figure 3: X-ray diffraction patterns of ceria nanoparticles at various synthesis conditions

(a) Re = 40 (b) Re = 245 and (c) Re = 325

High resolution TEM micrographs of the synthesized nanoparticles corresponding to the various flow conditions are shown in Figure 4. Planar spacings are detectable in these images and some representative regions are highlighted in the images. Planar spacings were also determined using XRD results in conjunction with the ICDD PDF-2 database. The lattice parameter was calculated using the formula:

$$a_0 = d\sqrt{(h^2 + k^2 + l^2)}$$

where d is the interplanar spacing and (hkl) are the Miller indices from the identified planes. The measured planar spacings based on the micrographs were compared with XRD results and the comparison is shown in Table 1.

Table 1: Comparison of lattice parameters for fluorite structured ceria

Re	Identified planes	D-spacing		Lattice parameter	
		from XRD	from HRTEM	from XRD	from HRTEM
40	(111)	0.312	0.315	0.540	0.546
	(200)	0.271	0.270	0.542	0.540
240	(111)	0.312	0.310	0.540	0.537
	(200)	0.271	0.280	0.542	0.560
325	(111)	0.312	0.315	0.540	0.546
	(200)	0.271	0.270	0.542	0.540

¹Data compared from XRD standard reference data from ICDD PDF-2 database

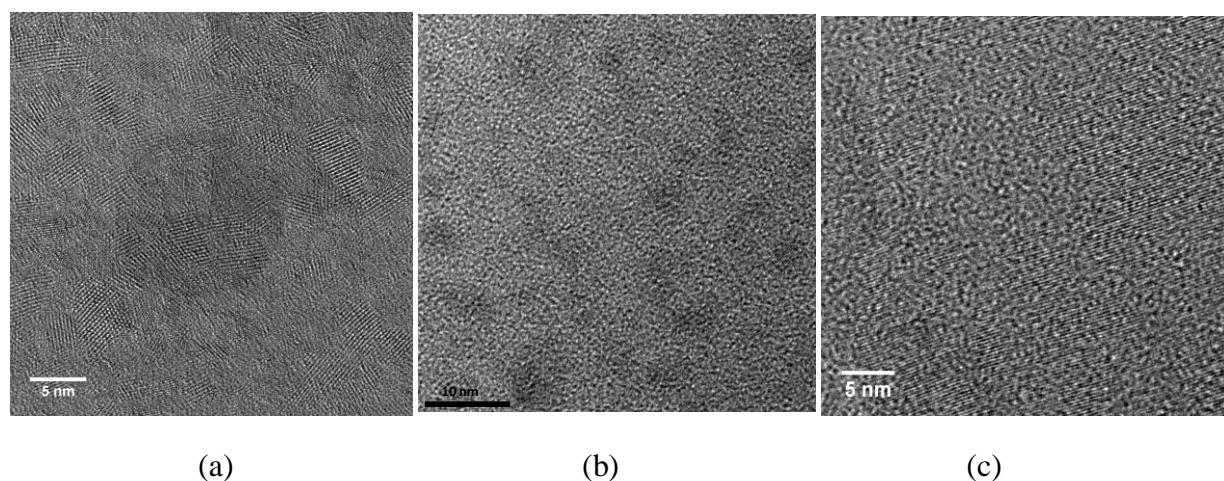


Figure 4: High resolution TEM images of ceria nanoparticles synthesized at (a) Re = 40 (b) Re = 245 and (c) Re = 325

It can be observed that the lattice parameters values are consistent between XRD and TEM for both the lowest and highest Re. At a Re of 245, the lattice parameter is found to be slightly higher compared to the equilibrium value of 0.541 nm for (200) plane. This difference can be attributed to a change in valency of cerium ion from +4 to +3 and to the small particle size. This behavior of size related change in valency has been first reported by Tsunekawa et al [43]. This finding would be confirmed in subsequent work.

The mean particle sizes were calculated based on TEM and XRD data and is summarized in table 2. Since the high resolution TEM images indicate that the particles are single crystalline, crystallite size calculated from the full width and half maxima (FWHM) of the ceria peaks would give the particle size. Also it is assumed that the contribution to peak broadening from strain in the nanoparticles is negligible. The Debye-Scherrer equation [44] is used to calculate the particle size using FWHM and is given by

$$B(2\theta) = \frac{K\lambda}{L \cos \theta}$$

Where B is the peak broadening from crystallites of size < 100 nm, K is the scherrer constant and is taken as 0.9 [45], λ is the wavelength of the x-ray beam and 2θ is the scattering angle.

Table 2: Nanoparticle size comparison

Re	Particle size (Mean \pm SD)	
	nm	
	from XRD	from TEM
40	20.7 \pm 3.5	-
240	9.6 \pm 1.5	7.59 \pm 5.54
325	14.7 \pm 6.4	15.03 \pm 4.73

Electron microprobe analysis using WDS was carried out to identify the composition of the precipitated nanoparticles and thereby confirm their stoichiometry. This was carried out for nanoparticles synthesized at Re of 245 and 325. The sample pertaining to Re 40 could not be satisfactorily characterized in WDS owing to the presence of the TEA complex leading to an increase in complexity of measurement. Several milligrams of the nanoparticles were synthesized and used to form a loosely bound film on glass substrate. The thickness, and hence the amount of nanoparticles, were adjusted to remove substrate effects during WDS probing. This is based on the interaction volume of the incident electron beam on the sample [46]. As shown in Figure 5, the interaction volume for the ceria sample was estimated using CASINO Monte Carlo simulation developed by Drouin et al [47]. It can be seen there is an interaction volume of approximately $1 \mu\text{m}^3$ at 20 keV incident energy. Hence it is expected that the composition information is collected from thousands of nanoparticles for each data point. The corresponding results for the compositional analysis are summarized in Tables 3 and 4 respectively.

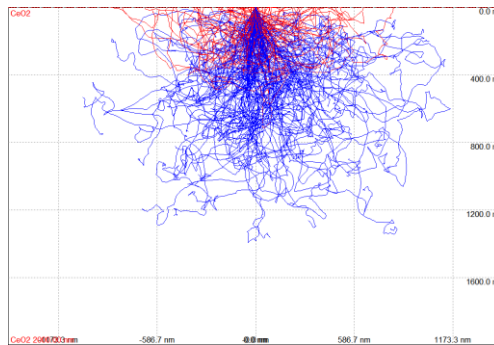


Figure 5. Monte-Carlo simulation of electron interaction volume in ceria sample

Table 3: Measured atomic percentage of ceria nanoparticles for case Re = 245

Point	Ce	O	O:Ce
-------	----	---	------

1	29.98	70.02	2.34
2	29.37	70.63	2.41
3	31.67	68.33	2.16
4	35.34	64.66	1.83
5	33.13	66.87	2.02
		Average	2.15

Table 4: Measured atomic percentage of ceria nanoparticles for case Re = 325

Point	Ce	O	O:Ce
1	31.66	68.34	2.16
2	38.19	61.81	1.62
3	28.87	71.13	2.46
4	38.22	61.78	1.62
5	32.34	67.66	2.09
		Average	1.99

On observing the stoichiometric ratio of oxygen to cerium, the higher flow rate shows an average stoichiometric ratio closer to the theoretical ratio of 2. This supplements earlier findings suggesting that better mixing leads to better nanoparticle stoichiometry. Also since the ratio is very close to 2, the contribution of cerium hydroxide to the stoichiometric ratio seems to be low suggesting that the volumetric percentage of cerium hydroxide in the sample is low. This is also consistent with the XRD results.

Simultaneous thermo gravimetric analysis and differential scanning calorimetry were performed on the samples to carry out extensive thermal analysis. The results are shown in figure 6. Comparing all the DSC results it can be observed that there is an exothermic peak in the 290°C – 320°C range. This can be attributed to conversion of Ce(OH)₃ to Ce₂O₃. This reaction is exothermic since it takes 1392 KJ/mol to break the three O-H bonds to form one Ce-O bond requiring 795 KJ/mol [48]. The weight loss is significant in all three samples around the same temperature consistent with loss of 3 moles of water formed for every 2 moles of cerium hydroxide. The possible reaction is



The start of amorphous to crystalline transformation can be observed for all samples around 600°C based on the DSC results. The heat flow required decreases with increasing Re again reinforcing the findings from XRD where higher Re implies higher crystallinity. An endothermic dip is also observed for these samples centered around 1000°C for (b) and 930°C for (c). This could be possibly be attributed to sintering of the nanoparticles. The peak at 900°C for (a) could result from the loss of carbon from the cerium-TEA complex. Again at 1185°C an endothermic peak suggests possible transition of CeO₂ to Ce₂O₃ under inert atmosphere through loss of oxygen for (a) and (c). A similar transition has been reported by Zhou et al at 1200°C [49]. The corresponding weight loss is observed to initiate at 1100°C for both (a) and (c). This transition is

not clearly observed for (b) and it is possible that the transition overlaps with the huge endothermic dip associated with sintering.

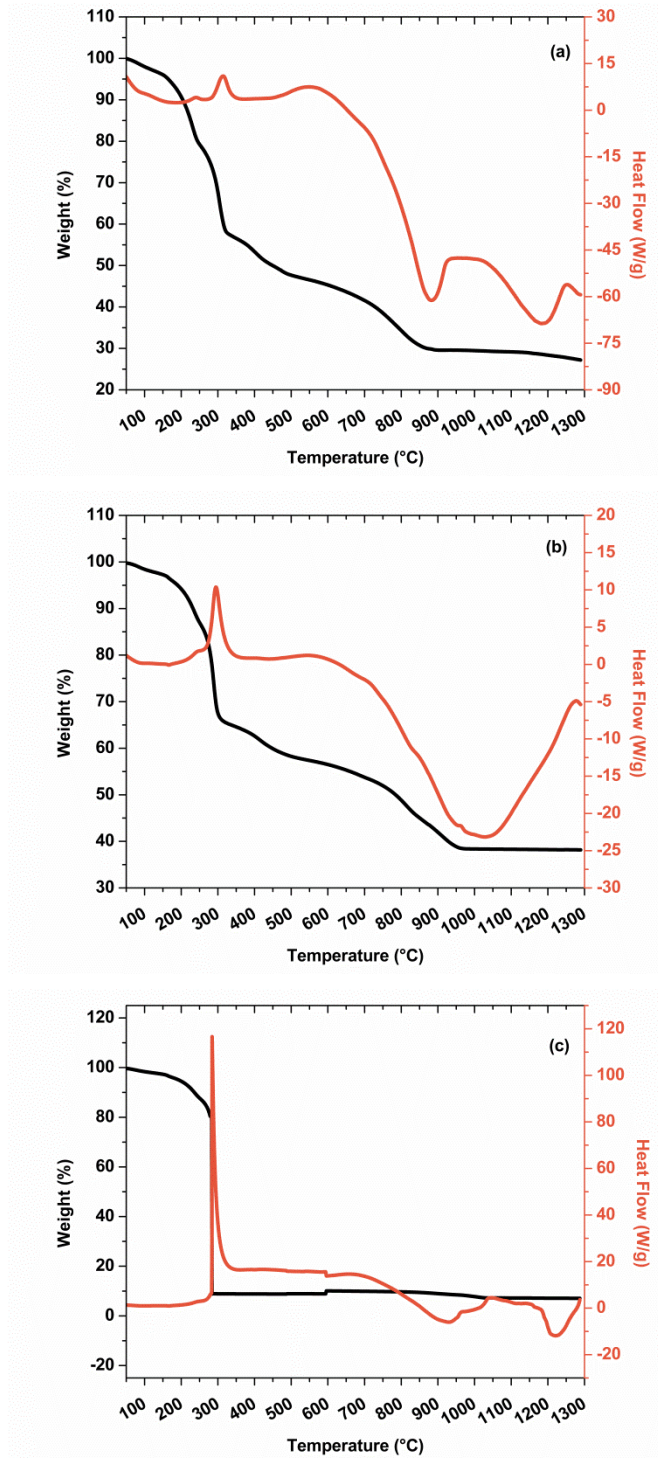


Figure 6: Simultaneous TGA/DSC results for a)Re = 40, b)Re = 245 and c) Re = 325

A summary of the particle sizes and shapes used for various applications of ceria NPs is shown in Table 5. This table suggests that nanoparticles synthesized in this paper could be useful as a sintering aid or in chemical mechanical planarization.

Table 5: Ceria nanoparticle characteristics based on application

Ref	Application	Typical size (nm)	Desired shape
[3, 50, 51]	Chemical Mechanical Planarization	5 - 100	Rounded, spherical
[4, 52]	Radical Scavenger	3 - 5	Faceted
[8, 12]	Fuel Cell	5 - 40	Cubical
[53, 54]	Catalyst	10 - 30	Octahedral
[55, 56]	Sintering aid	10 - 50	Spherical

Conclusions

In this research, a new synthesis route for ceria nanoparticle precipitation was demonstrated using engulfment flow conditions within a microchannel static T-mixer. NaOH was used to increase the rate of pH change, TEA was used to assist in the conversion of Ce^{+3} to Ce^{+4} and to help control agglomeration and IPA was used to provide better control over agglomeration. Several conclusions were drawn as a result of this research. First, using the chemistry and setup outlined in this paper, the flow regime used for nanoparticle synthesis, as dictated by the Re, was found to affect the attributes of the nanoparticles synthesized. Specifically, results show that the better mixing conditions due to flow engulfment with the static T-mixer lead to better stoichiometry and better crystallinity as well as better utilization of the reactants. Further, the average particle size was found to be larger under full engulfment flow (15.0 ± 4.7 nm) suggesting that better mixing may also lead to faster nucleation and growth in cerium oxide. Also, the ceria nanoparticle shape was found to be spherical and rounded under engulfment flow which is well-suited for applications in sintering and chemical mechanical planarization. Finally, despite the possibility that the enhanced advection under engulfment flow conditions could lead to greater agglomeration, nanoparticles produced under engulfment flow were found to be well dispersed with no agglomeration.

Acknowledgements

This material is based upon work supported by the National Science Foundation under Grant No. 0654434. The authors would like to acknowledge the support of instrumentation equipment within the Microproducts Breakthrough Institute, Corvallis, USA by the Murdock Charitable Trust (2010004). The authors would also like to thank Dr. Tom Tseng, alumni of our research group, for his prior work which provided insight into the direction of the current research. The authors would also like to thank Daniel Peterson, PhD student and Anna Garrison, Faculty Research Associate both at Oregon State University for their guidance and insightful discussions on the CFD results.

References

- [1] Izu, N., Shin, W., Murayama, N., and Kanzaki, S., 2002, "Resistive oxygen gas sensors based on CeO₂ fine powder prepared using mist pyrolysis," *Sens. Actuators, B*, 87(1), pp. 95-98.
- [2] Chen, P.-L., and Chen, I. W., 1993, "Reactive Cerium(IV) Oxide Powders by the Homogeneous Precipitation Method," *J. Am. Ceram. Soc.*, 76(6), pp. 1577-1583.
- [3] Yang, J. C., Kim, H.-j., and Kim, T., 2010, "Study of Polishing Characteristics of Monodisperse Ceria Abrasive in Chemical Mechanical Planarization," *J. Electrochem. Soc.*, 157(3), p. H235.
- [4] Karakoti, A. S., Singh, S., Kumar, A., Malinska, M., Kuchibhatla, S. V. N. T., Wozniak, K., Self, W. T., and Seal, S., 2009, "PEGylated Nanoceria as Radical Scavenger with Tunable Redox Chemistry," *J. Am. Chem. Soc.*, 131(40), pp. 14144-14145.
- [5] Yan, B., and Zhu, H., 2008, "Controlled synthesis of CeO₂ nanoparticles using novel amphiphilic cerium complex precursors," *J. Nanopart. Res.*, 10(8), pp. 1279-1285.
- [6] Quinelato, A., 2000, "Effect of ceria content on the sintering of ZrO₂ based ceramics synthesized from a polymeric precursor," *J. Eur. Ceram. Soc.*, 20(8), pp. 1077-1084.
- [7] Kumar, A., Babu, S., Karakoti, A. S., Schulte, A., and Seal, S., 2009, "Luminescence Properties of Europium-Doped Cerium Oxide Nanoparticles: Role of Vacancy and Oxidation States," *Langmuir*, 25(18), pp. 10998-11007.
- [8] Rebellato, J., Natile, M. M., and Glisenti, A., 2008, "Influence of the synthesis procedure on the properties and reactivity of nanostructured ceria powders," *Appl. Catal., A*, 339(2), pp. 108-120.
- [9] Yabe, S., and Sato, T., 2003, "Cerium oxide for sunscreen cosmetics," *J. Solid State Chem.*, 171(1-2), pp. 7-11.
- [10] Chen, J.-C., Chen, W.-C., Tien, Y.-C., and Shih, C.-J., 2010, "Effect of calcination temperature on the crystallite growth of cerium oxide nano-powders prepared by the co-precipitation process," *J. Alloys Compd.*, 496(1-2), pp. 364-369.
- [11] Phoka, S., Laokul, P., Swatsitang, E., Promarak, V., Seraphin, S., and Maensiri, S., 2009, "Synthesis, structural and optical properties of CeO₂ nanoparticles synthesized by a simple polyvinyl pyrrolidone (PVP) solution route," *Mater. Chem. Phys.*, 115(1), pp. 423-428.
- [12] Mai, H.-X., Sun, L.-D., Zhang, Y.-W., Si, R., Feng, W., Zhang, H.-P., Liu, H.-C., and Yan, C.-H., 2005, "Shape-Selective Synthesis and Oxygen Storage Behavior of Ceria Nanopolyhedra, Nanorods, and Nanocubes," *J. Phys. Chem. B*, 109(51), pp. 24380-24385.
- [13] Wang, T., and Sun, D., 2008, "Preparation and characterization of nanometer-scale powders ceria by electrochemical deposition method," *Mater. Res. Bull.*, 43(7), pp. 1754-1760.
- [14] Yin, L., Wang, Y., Pang, G., Koltypin, Y., and Gedanken, A., 2002, "Sonochemical Synthesis of Cerium Oxide Nanoparticles--Effect of Additives and Quantum Size Effect," *J. Colloid Interface Sci.*, 246(1), pp. 78-84.
- [15] Drobot, D., Chub, A., Voronov, V., Fedorov, P., Ivanov, V., and Polezhaeva, O., 2008, "Preparation of ceria nanoparticles," *Inorg. Mater.*, 44(8), pp. 853-855.
- [16] Zhou, X. D., Huebner, W., and Anderson, H. U., 2002, "Room-temperature homogeneous nucleation synthesis and thermal stability of nanometer single crystal CeO₂," *Appl. Phys. Lett.*, 80(20), p. 3814.
- [17] Schwarzer, H. C., and Peukert, W., 2004, "Tailoring particle size through nanoparticle precipitation," *Chem. Eng. Commun.*, 191(4), pp. 580-606.
- [18] Edel, J. B., Fortt, R., deMello, J. C., and deMello, A. J., 2002, "Microfluidic routes to the controlled production of nanoparticles," *Chem. Commun. (Cambridge, U. K.)*(10), pp. 1136-1137.
- [19] Chang, C. H., Paul, B. K., Remcho, V. T., Atre, S., and Hutchison, J. E., 2008, "Synthesis and post-processing of nanomaterials using microreaction technology," *J. Nanopart. Res.*, 10(6), pp. 965-980.
- [20] Joanicot, M., and Ajdari, A., 2005, "Droplet control for microfluidics," *Science*, 309(5736), p. 887.
- [21] Chang, C. H., Liu, S. H., Tennico, Y., Rundel, J. T., Remcho, V. T., Blackwell, E., Tseng, C. H., and Paul, B. K., "Progress Towards Chip-Based High-Throughput Dendrimer Synthesis," *Proc. International Conference on Microreaction Technology*, pp. 3011-3018.

- [22] Nakamura, H., Yamaguchi, Y., Miyazaki, M., Maeda, H., Uehara, M., and Mulvaney, P., 2002, "Preparation of CdSe nanocrystals in a micro-flow-reactor," *Chem. Commun.*(23), pp. 2844-2845.
- [23] Chan, E. M., Mathies, R. A., and Alivisatos, A. P., 2003, "Size-controlled growth of CdSe nanocrystals in microfluidic reactors," *Nano Lett.*, 3(2), pp. 199-201.
- [24] Yen, B. K. H., Stott, N. E., Jensen, K. F., and Bawendi, M. G., 2003, "A continuous-flow microcapillary reactor for the preparation of a size series of CdSe nanocrystals," *Adv. Mater. (Weinheim, Ger.)*, 15(21), pp. 1858-1862.
- [25] Krishnadasan, S., Tovilla, J., and Vilar, R., 2004, "On-line analysis of CdSe nanoparticle formation in a continuous flow chip-based microreactor," *J. Mater. Chem.*, 14(17), pp. 2655-2660.
- [26] Tseng, C., and Paul, B., 2007, "Comparison of batch mixing and micromixing approaches in the synthesis and deposition of ceria nanoparticles," *Transactions of NAMRI*, 35.
- [27] Engler, M., Kockmann, N., Kiefer, T., and Woias, P., 2004, "Numerical and experimental investigations on liquid mixing in static micromixers," *Chem. Eng. J.*, 101(1-3), pp. 315-322.
- [28] Kockmann, N., 2007, *Transport phenomena in micro process engineering*, Springer Verlag.
- [29] Wong, S., Ward, M., and Wharton, C., 2004, "Micro T-mixer as a rapid mixing micromixer," *Sens. Actuators, B*, 100(3), pp. 359-379.
- [30] Soleymani, A., Yousefi, H., Ratchananusorn, W., and Turunen, I., 2010, "Pressure drop in micro T-mixers," *J. Micromech. Microeng.*, 20(1), p. 015029.
- [31] Kockmann, N., Kastner, J., and Woias, P., 2008, "Reactive particle precipitation in liquid microchannel flow," *Chem. Eng. J.*, 135, pp. S110-S116.
- [32] Grundemann, L., Fischer, N., and Scholl, S., 2009, "From Macro Batch to Micro conti Manufacturing: A New Eco Friendly Production Process for Writing Ink Employing Micro process Engineering," *Chem. Eng. Technol.*, 32(11), pp. 1748-1756.
- [33] Schwarzer, H. C., and Peukert, W., 2004, "Combined experimental/numerical study on the precipitation of nanoparticles," *AIChE J.*, 50(12), pp. 3234-3247.
- [34] Azouani, R., Michau, A., Hassouni, K., Chhor, K., Bocquet, J. F., Vignes, J. L., and Kanaev, A., 2010, "Elaboration of pure and doped TiO₂ nanoparticles in sol-gel reactor with turbulent micromixing: Application to nanocoatings and photocatalysis," *Chem. Eng. Res. Des.*, 88(9), pp. 1123-1130.
- [35] Telib, H., Manhart, M., and Iollo, A., 2004, "Analysis and low-order modeling of the inhomogeneous transitional flow inside a T-mixer," *Phys. Fluids*, 16, p. 2717.
- [36] Schwarzer, H. C., and Peukert, W., 2002, "Experimental investigation into the influence of mixing on nanoparticle precipitation," *Chem. Eng. Technol.*, 25(6), pp. 657-661.
- [37] Liu, L., and Xu, J., 2011, "A study of the erosion–corrosion behavior of nano-Cr₂O₃ particles reinforced Ni-based composite alloying layer in aqueous slurry environment," *Vacuum*, 85(6), pp. 687-700.
- [38] Mullin, J. W., 2001, *Crystallization*, Butterworth-Heinemann.
- [39] Li, M., Zhang, R., Zhang, H., Feng, W., and Liu, X., 2010, "Synthesis, structural and magnetic properties of CeO₂ nanoparticles," *Micro & Nano Letters*, 5(2), p. 95.
- [40] Liu, K., and Zhong, M., 2010, "Synthesis of monodispersed nanosized CeO₂ by hydrolysis of the cerium complex precursor," *J. Rare Earth.*, 28(5), pp. 680-683.
- [41] Pati, R. K., Lee, I. C., Gaskell, K. J., and Ehrman, S. H., 2008, "Precipitation of Nanocrystalline CeO₂ Using Triethanolamine," *Langmuir*, 25(1), pp. 67-70.
- [42] He, B. B., 2011, *Two-dimensional X-Ray Diffraction*, John Wiley & Sons.
- [43] Tsunekawa, S., Ishikawa, K., Li, Z. Q., Kawazoe, Y., and Kasuya, A., 2000, "Origin of Anomalous Lattice Expansion in Oxide Nanoparticles," *Phys. Rev. Lett.*, 85(16), p. 3440.
- [44] Scherrer, P., 1918, "Bestimmung der Größe und der inneren Struktur von Kolloidteilchen mittels Röntgenstrahlen," *Nachr. Ges. Wiss. Göttingen*, 26, pp. 98-100.

- [45] Langford, J. I., and Wilson, A., 1978, "Scherrer after sixty years: a survey and some new results in the determination of crystallite size," *J. Appl. Crystallogr.*, 11(2), pp. 102-113.
- [46] Williams, D. B., and Carter, C. B., 2009, "The Transmission Electron Microscope," *Transmission Electron Microscopy*, pp. 3-22.
- [47] Drouin, D., Couture, A. R., Joly, D., Tastet, X., Aimez, V., and Gauvin, R., 2007, "CASINO V2. 42—A Fast and Easy-to-use Modeling Tool for Scanning Electron Microscopy and Microanalysis Users," *Scanning*, 29(3), pp. 92-101.
- [48] Wilcox, D., and Bromley, L., 1963, "Computer estimation of heat and free energy of formation for simple inorganic compounds," *Industrial & Engineering Chemistry*, 55(7), pp. 32-39.
- [49] Zhou, Y., and Rahaman, M., 1993, "Hydrothermal synthesis and sintering of ultrafine CeO₂ powders," *J. Mater. Res.*, 8(07), pp. 1680-1686.
- [50] Zhang, Z., Liu, W., Zhu, J., and Song, Z., 2010, "Synthesis, characterization of ceria-coated silica particles and their chemical mechanical polishing performance on glass substrate," *Appl. Surf. Sci.*, 257(5), pp. 1750-1755.
- [51] Armini, S., Burtovyy, R., Moinpour, M., Luzinov, I., Messemaeker, J. D., Whelan, C. M., and Maex, K., 2008, "Interaction Forces Between a Glass Surface and Ceria-Modified PMMA-Based Abrasives for CMP Measured by Colloidal Probe AFM," *J. Electrochem. Soc.*, 155(4), pp. H218-H223.
- [52] Kar, S., Patel, C., and Santra, S., 2009, "Direct Room Temperature Synthesis of Valence State Engineered Ultra-Small Ceria Nanoparticles: Investigation on the Role of Ethylenediamine as a Capping Agent," *The Journal of Physical Chemistry C*, 113(12), pp. 4862-4867.
- [53] Tan, J. P. Y., Tan, H. R., Boothroyd, C., Foo, Y. L., He, C. B., and Lin, M., 2011, "Three-Dimensional Structure of CeO₂ Nanocrystals," *The Journal of Physical Chemistry C*, 115(9), pp. 3544-3551.
- [54] Laosiripojana, N., and Assabumrungrat, S., 2011, "Conversion of poisonous methanethiol to hydrogen-rich gas by chemisorption/reforming over nano-scale CeO₂: The use of CeO₂ as catalyst coating material," *Applied Catalysis B: Environmental*, 102(1-2), pp. 267-275.
- [55] Yang, Y., Wang, Y., Wang, Z., Liu, G., and Tian, W., 2008, "Preparation and sintering behaviour of nanostructured alumina/titania composite powders modified with nano-dopants," *Materials Science and Engineering: A*, 490(1-2), pp. 457-464.
- [56] Muroi, M., Trotter, G., McCormick, P. G., Kawahara, M., and Tokita, M., 2008, "Preparation of nano-grained zirconia ceramics by low-temperature, low-pressure spark plasma sintering," *J. Mater. Sci.*, 43(19), pp. 6376-6384.